PLOS | PATHOGENS

RESEARCH ARTICLE

Microbial Community Composition Impacts Pathogen Iron Availability during Polymicrobial Infection

Apollo Stacy, Nader Abraham, Peter Jorth¤, Marvin Whiteley*

Department of Molecular Biosciences, Institute of Cellular and Molecular Biology, John Ring LaMontagne Center for Infectious Disease, The University of Texas at Austin, Austin, TX United States of America

¤ Current address: Division of Biology and Biological Engineering, California Institute of Technology, Pasadena, CA
* mwhiteley@austin.utexas.edu

Citation: Stacy A, Abraham N, Jorth P, Whiteley M (2016) Microbial Community Composition Impacts Pathogen Iron Availability during Polymicrobial Infection. PLoS Pathog 12(12): e1006084. doi:10.1371/journal.ppat.1006084

Editor: Alan R. Hauser, Northwestern University, UNITED STATES

Received: September 22, 2016

Accepted: November 21, 2016

Published: December 14, 2016

Data Availability Statement: All RNA-seq and ChIP-seq files are available from the National Center for Biotechnology Information Sequence Read Archive (accession numbers SRP081045 and SRP093165).

Funding: This work was supported by National Institutes of Health Grants R01DE023193 (to MW) and F31DE024931 (to AS). MW is a Burroughs Wellcome Investigator in the Pathogenesis of Infectious Disease. The funders had no role in study design, data collection and analysis, decision to publish, or preparation of the manuscript.

Abstract

Iron is an essential nutrient for bacterial pathogenesis, but in the host, iron is tightly sequestered, limiting its availability for bacterial growth. Although this is an important arm of host immunity, most studies examine how bacteria respond to iron restriction in laboratory rather than host settings, where the microbiome can potentially alter pathogen strategies for acquiring iron. One of the most important transcriptional regulators controlling bacterial iron homeostasis is Fur. Here we used a combination of RNA-seq and chromatin immunoprecipitation (ChIP)-seq to characterize the iron-restricted and Fur regulons of the biofilm-forming opportunistic pathogen *Aggregatibacter actinomycetemcomitans*. We discovered that iron restriction and Fur regulate 4% and 3.5% of the genome, respectively. While most genes in these regulons were related to iron uptake and metabolism, we found that Fur also directly regulates the biofilm-dispersing enzyme Dispersin B, allowing *A. actinomycetemcomitans* to escape from iron-scarce environments. We then leveraged these datasets to assess the availability of iron to *A. actinomycetemcomitans* in its primary infection sites, abscesses and the oral cavity. We found that *A. actinomycetemcomitans* is not restricted for iron in a murine abscess mono-infection, but becomes restricted for iron upon co-infection with the oral commensal *Streptococcus gordonii*. Furthermore, in the transition from health to disease in human gum infection, *A. actinomycetemcomitans* also becomes restricted for iron. These results suggest that host iron availability is heterogeneous and dependent on the infecting bacterial community.

Author Summary

One of the most well-studied phenomena in microbiology is nutritional immunity, or how the host withholds nutrients such as iron to combat infection. As part of this, researchers have characterized how many pathogens respond to iron restriction. However, these studies are often conducted in laboratory media rather than the host. As a result, they overlook how the host environment, such as its microbiome, might alter

Competing Interests: The authors have declared that no competing interests exist.

pathogen behavior regarding iron during infection. To address this gap, we used an opportunistic pathogen that causes abscess and oral cavity infections. We defined how it responds to iron restriction *in vitro* and then used this data to assess its iron status *in vivo*. Our results show that in mono-culture abscesses the pathogen is not starved for iron but in co-culture abscesses and multispecies gum disease it is starved for iron. Therefore, host environments are not uniformly restricted for iron, and the microbiome can modulate iron availability to pathogens.

Introduction

In 1944, researchers Schade and Caroline found that by adding egg whites to cultures of various microorganisms, they could stunt microbial growth. Remarkably, they could only relieve this inhibition by supplementing the cultures with iron [1]. This was the first suggestion that iron, an essential nutrient for most microbes, is withheld by the host as a means to restrict infection. Since then, an entire field has emerged on the role of iron in host immunity [2–6].

Most bacteria require at least 0.3–4 μM iron to grow [2]. Pathogens therefore meet a significant hurdle when they infect the human body, where most iron is sequestered. Inside cells, iron is bound by proteins such as hemoglobin and ferritin, and outside cells, iron is bound by proteins such as transferrin and lactoferrin [7]. As a result, free ionic iron is present in human fluids at only 10^{-12} μM [3], over 11 orders of magnitude below that needed by bacteria. Thus, compromises to "nutritional immunity" can greatly increase vulnerability to infection. Demonstrating this, patients with hyperferremia (iron overload) are more prone to infection, and supplementation of mammals with iron has been shown to enhance the virulence of microbial pathogens [4].

In addition to host measures, acquiring iron is made challenging because under oxidizing conditions, most iron is ferric (in the 3+ oxidation state), which is insoluble and limited in bioavailability [8]. Bacteria can circumvent these barriers by either releasing siderophore molecules that bind ferric iron with high affinity and return it to the cell or by displaying surface receptors that bind iron directly [9]. These strategies, however, must also be tightly regulated because excess iron is toxic [10]. Many bacteria regulate iron acquisition with the Ferric Uptake Regulator (Fur), a transcriptional regulator that alters gene expression in response to intracellular iron levels [11]. In general, holo-Fur (Fur bound to Fe^{2+}) represses gene expression, whereas apo-Fur (Fur not bound to Fe^{2+}) de-represses gene expression. Besides iron transport, Fur can also control many other aspects of bacterial physiology and behavior, including toxin production, stress resistance, and biofilm formation [11].

While most nutritional immunity studies center on the interaction between host and pathogen, polymicrobial interactions between pathogens and the host microbiota can also affect the success of pathogens in acquiring iron, either through competition [12, 13] or cooperation [14–16]. One of the most common infectious diseases, periodontitis (gum disease), is also influenced by iron [17–19]. Periodontitis is caused by the multispecies biofilm community that inhabits the gingival crevice, the pocket between the gum and tooth [20]. This site is partially anaerobic [21] and bathed in a serum exudate known as crevicular fluid. Crevicular fluid contains many potential iron sources for microbial growth including transferrin, lactoferrin, hemoglobin, and inorganic iron [22]. In healthy serum, the average total iron concentration is ~1 mg/l, whereas in periodontal crevicular fluid it increases to ~5 mg/l [22]. Although this suggests that iron is more bioavailable in disease, one of the most highly upregulated microbial community functions in human periodontitis is iron transport [23], suggesting instead that

iron is limited. The bioavailability of iron in periodontitis is therefore unclear and may depend on multiple factors.

An important member of oral microbial communities is the Gram-negative bacterium *Aggregatibacter actinomycetemcomitans*, an opportunistic pathogen associated with aggressive periodontitis. Notably, *A. actinomycetemcomitans* not only infects the oral cavity but can also spread throughout the body to cause abscesses [24]. In regards to iron sources, *A. actinomycetemcomitans* can use ferrous (Fe^{2+}) iron, ferric (Fe^{3+}) iron, and hemoglobin but not transferrin or lactoferrin [25–27]. Like most pathogens, the ability of *A. actinomycetemcomitans* to access one of these iron sources critically determines its virulence [28, 29]. Despite this, only a few iron acquisition systems in *A. actinomycetemcomitans* have been characterized. These systems directly bind and transport iron [25–27] since *A. actinomycetemcomitans* cannot make siderophores [25], and many of them are controlled by the *A. actinomycetemcomitans* Fur homolog. However, outside these systems only a few targets of Fur in *A. actinomycetemcomitans* are known [30].

Despite the clear importance of iron to bacterial infection, we know virtually nothing about how *A. actinomycetemcomitans* acquires it *in vivo*. How does *A. actinomycetemcomitans* surmount iron restriction at its different infection sites? How does *A. actinomycetemcomitans* interact with other bacteria regarding iron? Most importantly, how does *A. actinomycetemcomitans* respond to iron restriction *in vivo* to optimize its growth and virulence? With these questions in mind, our primary goal was to comprehensively characterize the *A. actinomycetemcomitans* iron-restricted and Fur regulons. We then leveraged these datasets to assess the *A. actinomycetemcomitans* iron response in both murine and human polymicrobial infections to determine the impact of microbial community composition and disease status on iron availability.

Results/Discussion

The *A. actinomycetemcomitans* iron-restricted regulon

To characterize how *A. actinomycetemcomitans* responds to iron restriction, we performed RNA-seq to compare its gene expression between rich media and iron-chelated media (see Tables 1–2 in S1 Dataset for study design). Since *A. actinomycetemcomitans* does not grow planktonically, we grew it as colony biofilms. We also used anaerobic growth conditions since soluble Fe^{2+} predominates and can be readily chelated with 2,2'-dipyridyl to mimic iron-restricted conditions. In total we discovered 93 genes, representing 4% of the genome, which are differentially expressed in response to iron restriction (Table 3 in S1 Dataset). Of these, over twice as many were upregulated than downregulated, and upregulated genes generally had larger fold changes than downregulated genes (S1A Fig).

Most genes downregulated in iron-restricted conditions encoded components of the anaerobic electron transport chain (Fig 1), suggesting that iron restriction hinders *A. actinomycetemcomitans* anaerobic respiration. These downregulated genes included the Na^{+}-translocating NADH-quinone reductase [31], menaquinone biosynthesis [32], anaerobic respiratory reductases [33] as well as two major steps in pyruvate metabolism (Fig 1). The fact that many of these downregulated gene products contain iron suggests that restricting cellular iron usage is central to the *A. actinomycetemcomitans* iron starvation response. Supporting this, one of the most downregulated gene products in response to iron restriction was the iron storage protein ferritin (Fig 1).

Genes upregulated in response to iron restriction primarily encoded iron transporters and receptors. These include 5 inner membrane ABC transporters (including the characterized Afu [34] and Afe [35] systems), TonB [36], and 5 outer membrane TonB-dependent receptors

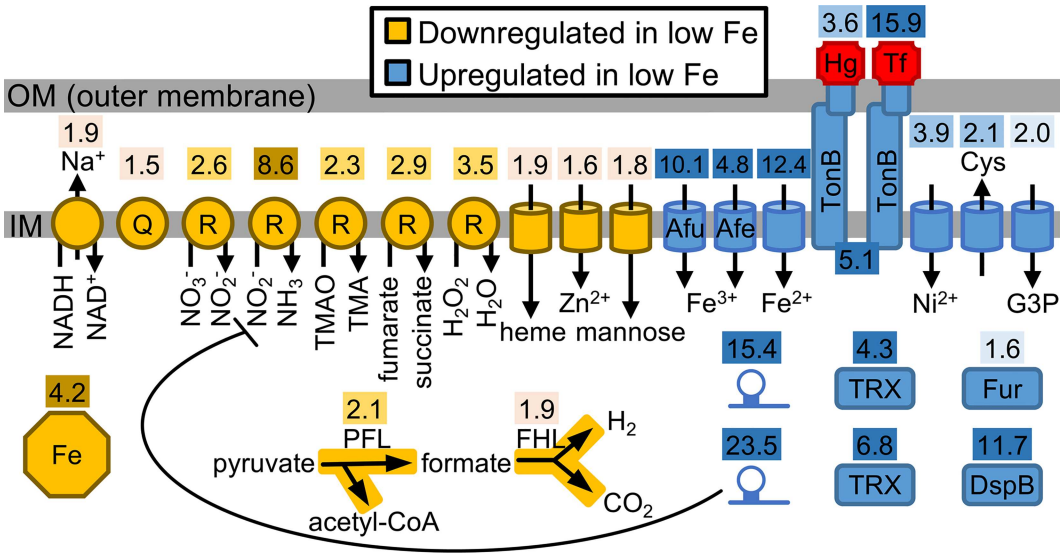

Fig 1. The *A. actinomycetemcomitans* iron-restricted regulon. Cellular processes differentially expressed by iron restriction. Shaded numbers above each process indicate fold change. 1.5–2.0 fold, light shade; >2.0–4.0 fold, medium shade; >4.0 fold, dark shade. Octagon, ferritin; Q, quinone; R, respiratory reductase; TMAO, trimethylamine N-oxide; TMA, trimethylamine; PFL, pyruvate formate lyase; FHL, formate hydrogen lyase; Afu and Afe, characterized transporters; Hg, hemoglobin; Tf, transferrin; Cys, cysteine; G3P, glycerol-3-phosphate; hairpin, sRNA; TRX, thioredoxin; DspB, Dispersin B.

doi:10.1371/journal.ppat.1006084.g001

(Fig 1). Substrates of these systems included inorganic iron, ferric iron siderophores, hemoglobin, and transferrin. Transporters for metals besides iron–nickel and zinc–were also differentially expressed (Fig 1). Although the significance of these non-iron transporters is unclear, co-expression of nickel with iron transporters has been observed in other bacteria [37].

Other processes upregulated in response to iron restriction included cysteine export by the CydDC transporter [38] (Fig 1). CydDC is required for the assembly of cytochrome *bd* (CydAB), and as CydAB is the sole aerobic respiratory oxidase in *A. actinomycetemcomitans* [39], this suggests that aerobic respiration in *A. actinomycetemcomitans* is stimulated by iron restriction. This is noteworthy considering that most of the *A. actinomycetemcomitans* anaerobic respiratory reductases were repressed by iron restriction. *A. actinomycetemcomitans* therefore seems to equate iron restriction with the presence of oxygen. Supporting this, a transporter for glycerol-3-phosphate, a carbon source that can only be catabolized by respiration [40], and 2 thioredoxins, implicated in resisting oxidative stress from oxygen [41], were also more highly expressed under iron restriction (Fig 1).

The only differentially expressed non-coding genes were 2 small RNAs (sRNA) upregulated by iron restriction (Fig 1). One of these sRNA was homologous to an iron-regulated sRNA in *H. influenzae* [42], and like *H. influenzae*, this sRNA in *A. actinomycetemcomitans* was also predicted to target asparagine biosynthesis (P = 0.03, TargetRNA2). The other sRNA was predicted to target nitrite reductase (P = 0.05, TargetRNA2 [43]), one of the most downregulated gene products in response to iron restriction.

The *A. actinomycetemcomitans* Fur regulon

We next set out to characterize the *A. actinomycetemcomitans* Fur regulon with the goal of defining which iron-responsive genes were controlled by this transcriptional regulator. To do this, we used RNA-seq to compare gene expression of wild type *A. actinomycetemcomitans* to an isogenic Δ*fur* mutant (see Tables 1–2 in S1 Dataset for study design). Overall, we found that

386 genes, representing over 17% of the genome, were differentially expressed when Fur is absent, with slightly more genes activated than repressed (Table 3 in S1 Dataset). As expected, the Fur regulon extensively overlapped the iron-restricted regulon, with Fur-repressed genes mostly overlapping genes upregulated in iron-restricted conditions, and Fur-activated genes mostly overlapping genes downregulated in iron-restricted conditions (Table 4 in S1 Dataset). In total, the Fur regulon encompassed 70 of 93 genes in the iron-restricted regulon, indicating that as expected, Fur has a critical role in controlling *A. actinomycetemcomitans* iron homeostasis. Supporting this, all of the iron uptake systems that were upregulated in iron-restricted conditions were repressed by Fur, and all of the anaerobic respiratory reductases that were downregulated in iron-restricted conditions were activated by Fur (S1 Table).

Many Fur-activated genes were also related to carbon utilization (S1 Table). As these genes were not regulated by iron, we suspected that their control by Fur was due to indirect rather than direct regulatory changes. Supporting this, we identified 10 transcriptional regulators that were differentially expressed in the Δ*fur* mutant (S2A Fig). Furthermore, promoters of several Fur-activated genes contained a DNA binding motif for the cyclic AMP (cAMP) receptor protein (CRP) (S2B Fig), a regulator that alters gene expression in response to binding cAMP [44, 45]. As the CRP regulon in *A. actinomycetemcomitans* has been characterized [46], we could examine its overlap with the Fur regulon. This revealed that Fur-activated genes are enriched for both CRP-repressed ($P = 1 \times 10^{-11}$) and CRP-activated genes ($P = 3 \times 10^{-4}$, one-tailed Fisher's exact test) (Table 4 in S1 Dataset). These results show that Fur expands its control over gene expression by acting indirectly through other transcriptional regulators including CRP.

To gain a more in-depth understanding of the Fur regulon, we next used the KEGG resource [47] to reconstruct how Fur globally regulates *A. actinomycetemcomitans* metabolism (Fig 2, S1 Table). As Fur activity is essentially a proxy for cellular iron levels, this network could be interpreted as how *A. actinomycetemcomitans* metabolism might adapt to iron-restricted conditions. In general, we found that the Fur-activated regulon is metabolically diverse, encompassing several central metabolism and carbon utilization pathways. Central metabolism pathways activated by Fur included glycolysis, the pentose phosphate pathway, pyruvate metabolism, and the reductive TCA cycle, and carbon utilization pathways included those for ribose, ascorbate, citrate, gluconate, glycerol, and inositol.

In contrast, analogous pathways in the Fur-repressed regulon were much less diverse and suggest that iron-restricted *A. actinomycetemcomitans*, like other bacteria [48], primarily engages in fermentation, mediated by a D-lactate dehydrogenase and a zinc-dependent alcohol dehydrogenase. However, Fur both repressed and activated metabolic pathways related to amino acids, vitamins, and cofactors. For instance, chorismate (a precursor to aromatic amino acids) and serine biosynthesis were repressed by Fur, while tyrosine and serine transport were activated by Fur. Other processes regulated by Fur included autoinducer-2 (AI-2) signaling, toxin production, and biofilm formation. Specifically, the Lsr AI-2 transporter [49], leukotoxin [50], and tight adherence [51] pili that mediate surface attachment were activated by Fur, while cytolethal distending toxin [52] was repressed by Fur.

Iron and Fur regulate Dispersin B

Iron restriction also caused Fur-mediated upregulation of the gene encoding Dispersin B (DspB) (Fig 1, S1 Table), an enzyme produced by *A. actinomycetemcomitans* to disperse from biofilms [53]. Previously we showed that *dspB* transcription is increased during aerobic growth via the transcriptional regulator OxyR [54]; however, the fact that we performed our experiments under strictly anaerobic conditions suggests that *dspB* transcription is also controlled by iron in an oxygen-independent manner. Thus, we hypothesized that iron restriction would

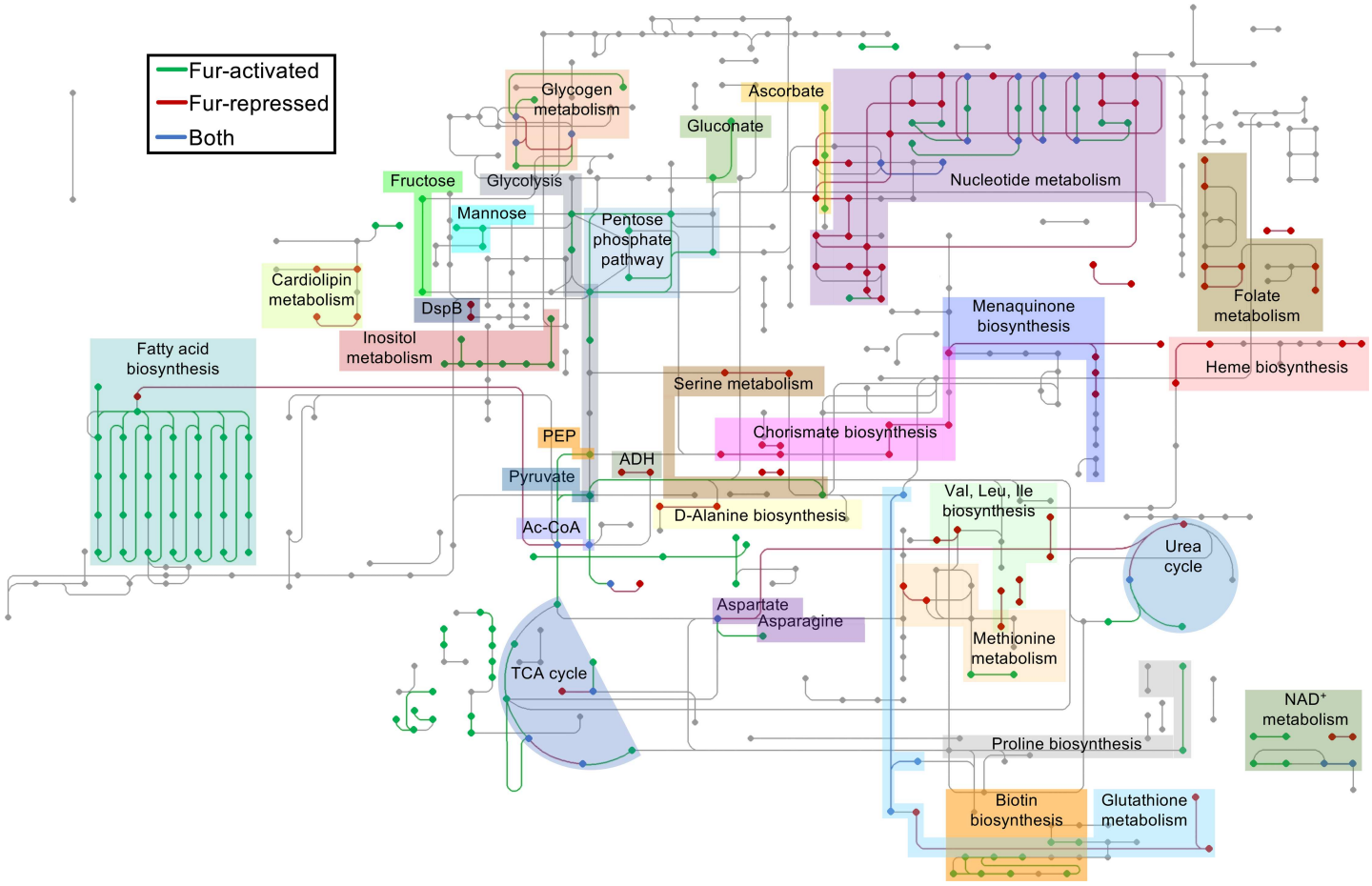

Fig 2. The *A. actinomycetemcomitans* Fur regulon. The metabolic network differentially expressed in the *Δfur* mutant. Legend: green, pathways downregulated in the *Δfur* mutant compared to the wild type (Fur-activated); red, pathways upregulated in the *Δfur* mutant compared to the wild type (Fur-repressed); blue, pathways mediated by both Fur-activated and -repressed genes. Dots and lines represent compounds and reactions, respectively. PEP, phosphoenolpyruvate; ADH, alcohol dehydrogenase; Ac-CoA, acetyl-CoA; TCA, tricarboxylic acid.

doi:10.1371/journal.ppat.1006084.g002

induce transcription of *dspB* in a Fur-dependent manner and subsequently lead to dispersal of *A. actinomycetemcomitans* from biofilms. To test this hypothesis, we first searched the *dspB* promoter for a Fur binding motif. This revealed a sequence that overlaps the *dspB* transcriptional start site and lies downstream of the reported [54] OxyR binding motif (Fig 3A). We then used a *dspB* promoter-*lacZ* transcriptional fusion to measure how *dspB* transcription is impacted by iron restriction. First we grew *A. actinomycetemcomitans* as colony biofilms under anaerobic conditions, and then to restrict iron, we transferred these biofilms to media containing an iron chelator. As expected, *A. actinomycetemcomitans* induced transcription of *dspB* >5 fold upon iron restriction, and we observed this effect in two different strains of *A. actinomycetemcomitans* (Fig 3B), 624 (the primary strain used in this study) and VT1169. Furthermore, this effect was iron-specific as addition of $FeSO_4$ to the chelated media abolished *dspB* induction (Fig 3B). We then tested the *Δfur* mutant under the same conditions and observed a >30 fold induction of *dspB* transcription. However, this induction occurred irrespective of iron levels (Fig 3B) confirming that Fur represses *dspB*. Genetic complementation of the *Δfur* mutant restored responsiveness to exogenous iron levels (Fig 3C) indicating that the response was specific to Fur.

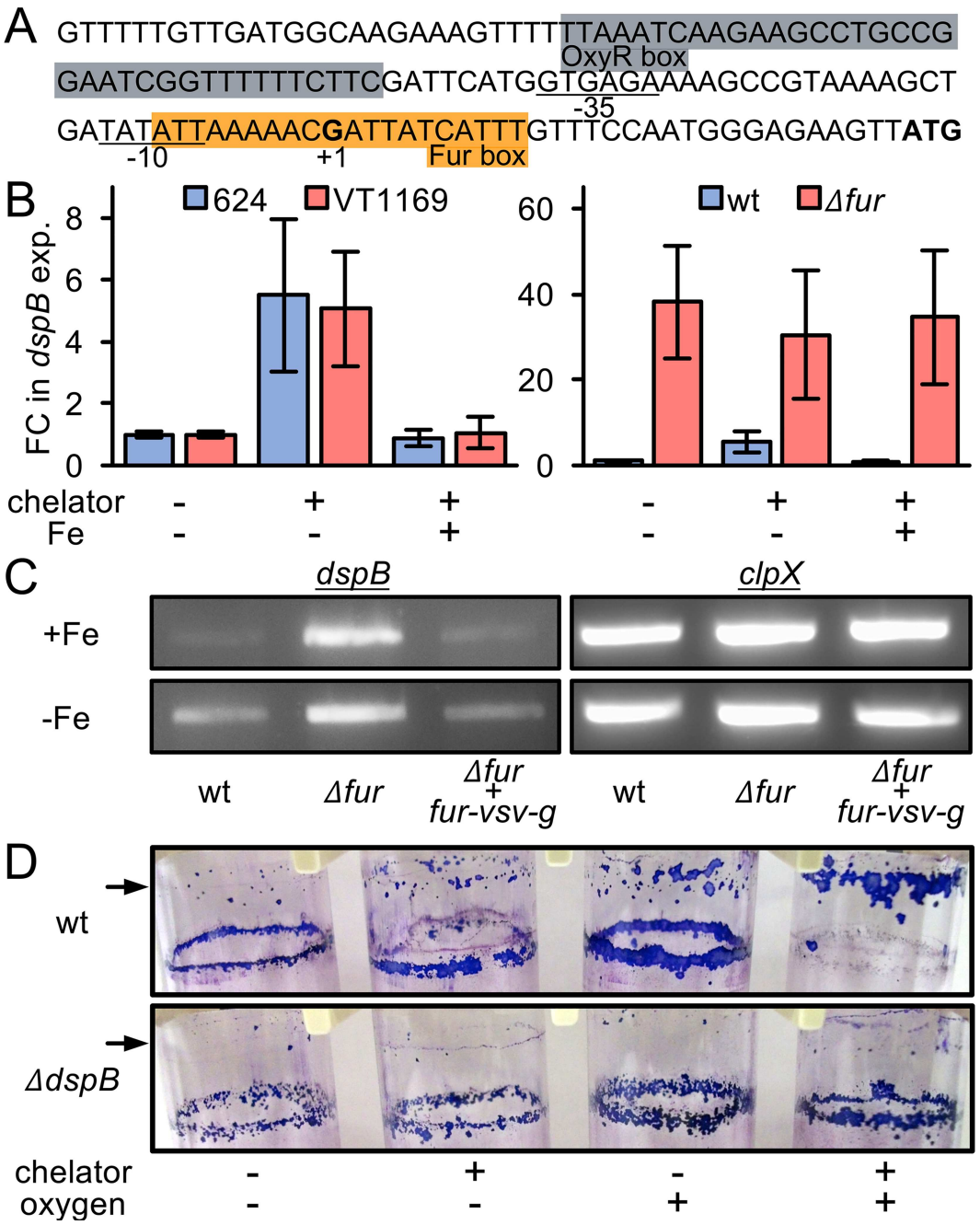

Fig 3. Iron and Fur regulate Dispersin B. (A) Structure of the *dspB* promoter. Gray, OxyR box; orange, Fur box; underlined, -35 and -10 regions; +1, transcriptional start site; bold, start codon. (B) *dspB* transcription in colony biofilms was measured using a *dspB* promoter-*lacZ* transcriptional fusion. Left panel: blue, *A. actinomycetemcomitans* strain 624; red, *A. actinomycetemcomitans* strain VT1169. Right panel: blue, *A. actinomycetemcomitans* strain 624 wild type (wt); red, *A. actinomycetemcomitans* strain 624 Δ*fur* (Δ*fur*). Chelator is 250 μM 2,2'-dipyridyl, and Fe is 250 μM $FeSO_4$. Y axis is fold change (FC) in *dspB* expression relative to no chelator (-chelator) and no $FeSO_4$ (-Fe) addition. Error bars represent standard deviation (n = 3). (C) *dspB* mRNA levels in colony biofilms was measured using reverse transcriptase PCR in iron-replete (+Fe) and iron-restricted (-Fe) conditions. *clpX* serves as a control that is not regulated by iron or Fur. Wild type (wt), Δ*fur* (Δ*fur*), Δ*fur* + *fur-vsv-g* (Δ*fur* genetically complemented with VSV-G tagged Fur). (D) Biofilm dispersal assay. A second, higher ring biofilm (indicated by arrow) indicates dispersal. The purple stain is crystal violet. Chelator is 250 μM 2,2'-dipyridyl; -oxygen is anaerobic growth; +oxygen is aerobic growth.

doi:10.1371/journal.ppat.1006084.g003

We next used a previously described biofilm dispersal assay [54] to test if iron restriction triggers *A. actinomycetemcomitans* biofilm dispersal. This assay takes advantage of the fact that when *A. actinomycetemcomitans* is grown with shaking in a glass test tube, it forms a "ring biofilm" on the test tube (Fig 3D). The assay works by first forming a ring biofilm in a low volume of media and then adding more media. If a second biofilm then forms above the first biofilm, dispersal has occurred. Using this assay, we found that *A. actinomycetemcomitans* can be induced to disperse from biofilms by adding an iron chelator (Fig 3D). Notably, biofilms dispersed even under anaerobic conditions. Although the assay is qualitative, we could also observe that iron-restricted biofilms dispersed even further in the presence of oxygen (Fig 3D). This suggests that iron restriction and aerobic growth conditions can work synergistically to promote biofilm dispersal. Together, these results show that, in addition to oxygen and OxyR, *dspB* is regulated by iron and Fur, and this regulation mediates *A. actinomycetemcomitans* biofilm dispersal in response to iron restriction.

The direct *A. actinomycetemcomitans* Fur regulon

One important drawback of our experimental approach for defining the Fur regulon is the inability to distinguish between direct and indirect gene regulation. We therefore used ChIP-seq to identify Fur binding sites (see Tables 1–2 in S1 Dataset for study design). To perform ChIP-seq, we complemented the *Δfur* mutant with a version of Fur tagged with the VSV-G epitope, allowing for immunoprecipitation. Importantly, VSV-G tagged Fur was expressed from its native promoter on a low-copy plasmid, and it genetically complemented the *Δfur* mutant (Fig 3C). In taking this approach, we hoped to prevent artefactual binding events that could arise from overexpression.

In total, we identified 67 promoter regions, representing 77 genes that are directly bound by Fur in either iron-replete or iron-restricted conditions. After accounting for potential operons, this total increased to 91 genes, revealing that Fur directly regulates 3.5% of the genome (Table 3 in S1 Dataset). To our surprise, only 41 of the 91 Fur-bound promoters were differentially controlled in iron-restricted conditions or in the *Δfur* mutant (S1C Fig). As this has been seen in other bacteria [55], this phenomenon may be more widespread than expected. Although RNA-seq suggested Fur activates as much as it represses gene expression (Table 3 in S1 Dataset), ChIP-seq revealed that Fur primarily represses gene expression (Table 6 in S1 Dataset), with over 4 times as many genes being directly repressed by Fur than activated. As expected, promoters directly bound by Fur contained a sequence similar to reported [37, 55] Fur binding motifs (Fig 4A).

In regards to function, many of the genes directly regulated by Fur were related to iron homeostasis as well as other metabolic processes (Fig 4B). Iron transporters directly regulated by Fur included the Afu ferric iron ABC transporter [34], 3 ferric iron siderophore transporters, TonB, and 5 TonB-dependent receptors, including those for hemoglobin and transferrin [26]. Interestingly, one ferric iron siderophore transporter was not differentially expressed in either iron-restricted conditions or in the *Δfur* mutant (Fig 4B). Other iron-related proteins directly regulated by Fur included ferritin and Fur itself, demonstrating that as in many other bacteria with Fur homologs [11], Fur in *A. actinomycetemcomitans* is autoregulated.

Metabolic processes directly regulated by Fur included glycerol transport, galactoside degradation, aromatic amino acid metabolism, glucose catabolism, uracil degradation, and the biosynthesis of NAD^+ and folate (Fig 4B). ChIP-seq also revealed that Fur controls both the biosynthesis and degradation of cAMP (Fig 4B), explaining the regulatory link we discovered between the Fur and CRP regulons (S2 Fig). Even though these two regulons were highly overlapping (Table 4 in S1 Dataset), CRP was not among the transcriptional regulators differentially

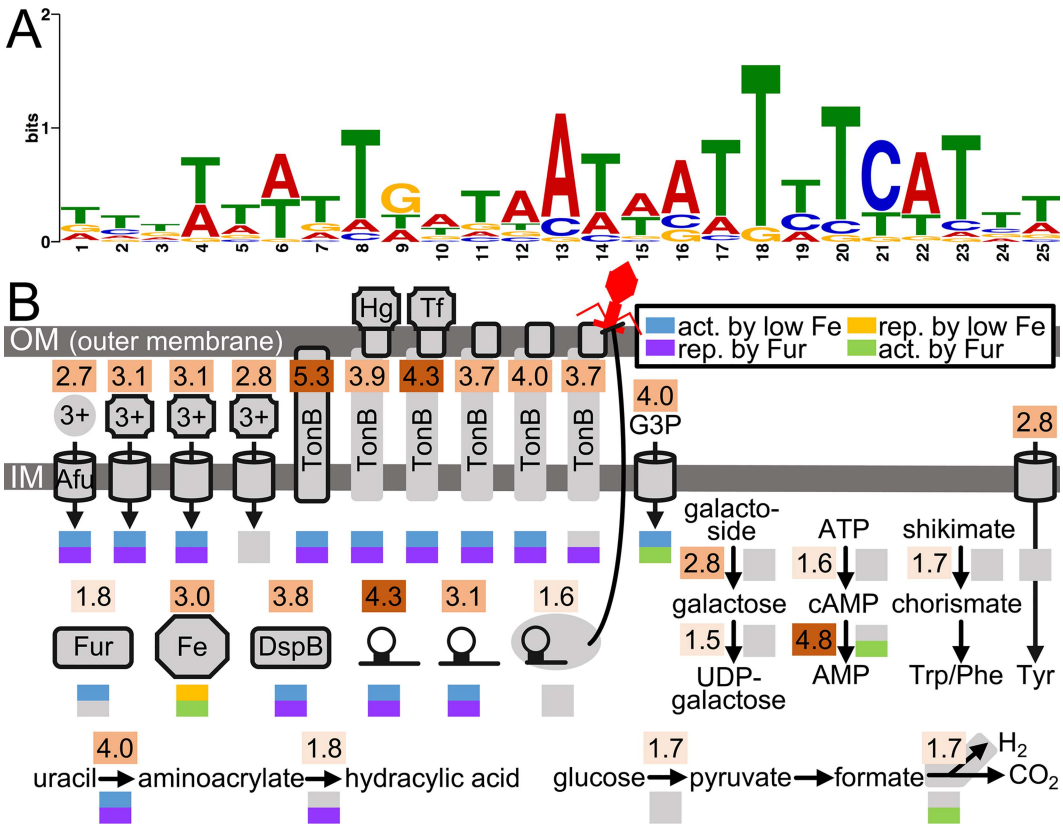

Fig 4. The *A. actinomycetemcomitans* direct Fur regulon. (A) Sequence logo representation of the Fur binding motif generated from all Fur-bound promoters (False Discovery Rate < 0.1) as outlined in Materials and Methods. The height of each base represents its frequency of occurrence. (B) Cellular processes directly regulated by Fur. Each process is encoded by a gene(s) whose promoter is bound by Fur. Shaded numbers above each process indicate fold enrichment of the ChIP to input DNA signal. 1.5–2.0 fold, light shade; >2.0–4.0 fold, medium shade; >4.0 fold, dark shade. Colored boxes below each process indicate transcriptional regulation by iron (blue or orange), Fur (purple or green), or neither (gray). Act. Is activated, and rep. is repressed. Afu, characterized transporter; 3+ in circle, free ferric iron; 3+ in square, ferric iron siderophore; Hg, hemoglobin; Tf, transferrin; octagon, ferritin; DspB, Dispersin B; hairpin, sRNA; hairpin in gray oval, CRISPR inhibiting a phage at the cell surface; G3P, glycerol-3-phosphate; cAMP, cyclic AMP; Trp, tryptophan; Phe, phenylalanine; Tyr, tyrosine.

doi:10.1371/journal.ppat.1006084.g004

expressed in the *Δfur* mutant (S2A Fig). This suggested control at the post-transcriptional level. As revealed by ChIP-seq, Fur exerts this control over CRP by regulating intracellular amounts of cAMP. Similar connections between Fur and CRP have been described in other bacteria [44, 45].

While most Fur-bound promoters were positioned ahead of coding genes, the direct Fur regulon also comprised 5 sRNA (Table 3 in S1 Dataset), including the 2 sRNA that we found are upregulated by iron restriction (Fig 4B). The promoters of 2 CRISPR-associated (*cas*) genes were also bound by Fur (Fig 4B). Though the promoter of the CRISPR itself was not bound by Fur, 2 other CRISPR in the genome were differentially expressed in the *Δfur* mutant (Table 3 in S1 Dataset). As there are a total of 3 CRISPR in our strain, the collective findings of our RNA- and ChIP-seq data suggest that Fur contributes to the regulation of all 3 CRISPR in the genome. One explanation for why *A. actinomycetemcomitans* evolved to regulate CRISPR with Fur is that surface-displayed iron receptors can serve as attachment sites for bacteriophages [56] (Fig 4B).

Finally, we found that Fur directly binds the *dspB* promoter, revealing that its upregulation in both iron-restricted conditions and the *Δfur* mutant (Fig 3) was due to direct de-repression

by Fur. Interestingly, we found that Fur also binds to a gene in the tight adherence pili locus. As RNA-seq showed that this locus is activated by Fur, this suggests a model where iron controls the entire *A. actinomycetemcomitans* biofilm cycle: in the absence of iron, Fur promotes biofilm dispersal by de-repressing Dispersin B (Fig 3), whereas in the presence of iron, Fur promotes surface attachment by activating the tight adherence pili. Altogether, our ChIP-seq dataset extended our understanding of the Fur regulon, beyond that provided by RNA-seq, and gave insight into Fur's complex role in not only iron transport but also cAMP biogenesis, viral defense, and biofilm formation.

The *A. actinomycetemcomitans* iron and Fur regulons in abscess infections

After characterizing the iron and Fur regulons *in vitro*, we next set out to leverage these datasets for assessing iron availability in *A. actinomycetemcomitans* infections. While *A. actinomycetemcomitans* is most widely associated with oral cavity infections, it can also spread systemically and cause abscesses in many parts of the body [24]. Like the oral cavity, abscesses are thought to be strong targets of host iron restriction [57] suggesting that *A. actinomycetemcomitans* is likely restricted for iron in the abscess. To test this, we used principle component analysis (PCA) to determine whether *A. actinomycetemcomitans* gene expression in the abscess (using a published dataset [58]) is more similar to its gene expression in biofilms on rich (Fe+) media or on iron-chelated (Fe-) media. To our surprise, the PCA showed that the abscess lies closer to Fe+ than Fe- biofilms (Fig 5A). To quantify this relationship, we used Spearman's correlation coefficient. This also showed that the abscess is more similar to Fe+ than Fe- biofilms (Fig 5B). We then repeated these analyses for genes in the Fur regulon, now comparing gene expression in the abscess to biofilms of the wild type and *Δfur* mutant. This showed that the abscess lies closer to and correlates better with the wild type than the *Δfur* mutant (S3 Fig). As gene expression in the *Δfur* mutant is essentially like that of iron-restricted wild type, the higher proximity of the abscess to the wild type suggests that gene expression within this infection better resembles that where iron is abundant than scarce. Together, these analyses indicate that *A. actinomycetemcomitans* is not restricted for iron in the abscess, contrasting our initial hypothesis.

To support this finding, we next decided to test the *Δfur* mutant in the abscess. In almost every pathogen and infection model tested, Fur is required for virulence [11]. Therefore, we reasoned that if iron is indeed not restricted in the abscess, Fur should not be required for *A. actinomycetemcomitans* virulence. As we anticipated, the *Δfur* mutant persisted just as well as the wild type in the abscess (Fig 5C), again indicating that *A. actinomycetemcomitans* does not face severe iron restriction in this host environment. As a final test, we also performed ChIP-seq on *A. actinomycetemcomitans* in the abscess, reasoning that we should be able to detect binding if iron is available. In total, we identified 18 promoters that are bound by Fur *in vivo* (Fig 5D). These promoters were a subset of the promoters that we identified are bound by Fur *in vitro*. Notably, the *in vivo*-bound promoters were enriched for promoters that are preferentially bound by Fur in the presence of iron ($P = 0.08$, one-tailed Fisher's exact test) (Fig 5D, Table 5 in S1 Dataset), reaffirming our conclusion that *A. actinomycetemcomitans* is not iron-restricted in the abscess.

One possible explanation for this result is that *A. actinomycetemcomitans* elicits an immune response that fails to fully sequester iron from the abscess. Alternatively, iron could be low but spatially heterogeneous in the abscess (S5A Fig), forming iron-rich 'patches' that locally promote *A. actinomycetemcomitans* colonization and growth. Supporting this, *A. actinomycetemcomitans* proliferates in the abscess as small (<10 μm across) cell aggregates [54]. Future

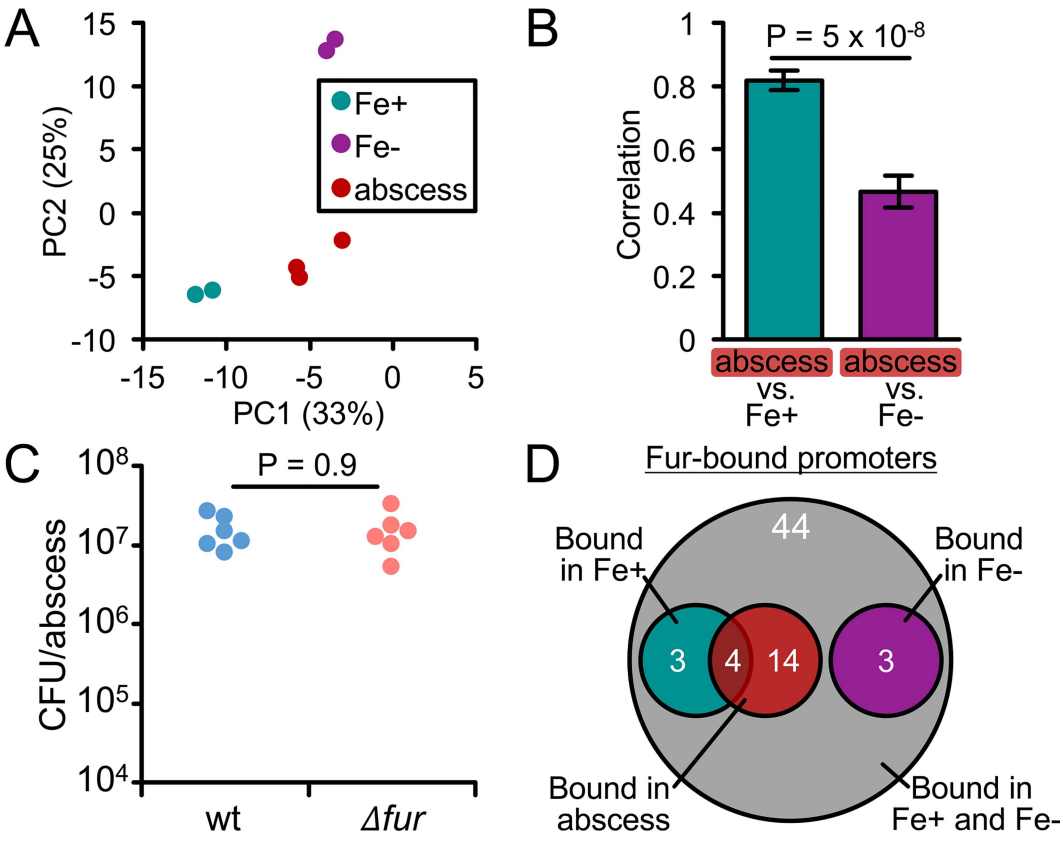

Fig 5. *A. actinomycetemcomitans* is not iron-restricted in murine abscess mono-infection. (A) Principal component analysis of the 93 genes regulated by iron. Each dot is a single replicate. Legend: Fe+, biofilm on rich media; Fe-, biofilm on iron-chelated media; abscess, wild-type abscess infection. Axes: Percentages are the amount of variation captured by each principal component. (B) Correlation analysis of the 93 genes regulated by iron. Spearman's rank correlation was determined by comparing gene expression in wild-type *A. actinomycetemcomitans* abscess infection to Fe+ and Fe- *in vitro* biofilms. Error bars represent standard deviation (n = 6 pairwise comparisons). Significance was determined using a 2-tailed t test. (C) Survival of the wild type (wt) and *Δfur* mutant in abscesses. Each dot is a single abscess (n = 2 biological replicates). Significance was determined using a Mann-Whitney U test. Y axis represents colony forming units (CFU) per abscess after 3 days post-infection. (D) Venn diagram showing the overlap between the *in vitro* and *in vivo* ChIP-seq results.

doi:10.1371/journal.ppat.1006084.g005

studies should therefore focus on examining the host response to *A. actinomycetemcomitans* using more direct means to quantitatively map iron levels, addressing the possibility that iron forms concentrated micron-scale patches and gradients in the abscess.

The *A. actinomycetemcomitans* iron and Fur regulons in abscess co-infections

As most pathogens cause infections as part of multispecies communities [59], we next sought to determine how co-infecting bacteria influence iron availability to *A. actinomycetemcomitans in vivo*. In the oral cavity, some of the most prevalent bacteria are Gram-positive streptococci [60]. Previously, we showed that intricate metabolic interactions, both cooperative [39] and competitive [54], with *Streptococcus gordonii* enhance *A. actinomycetemcomitans* virulence during abscess co-infection. Therefore, we conducted RNA-seq on abscesses co-infected with *A. actinomycetemcomitans* and *S. gordonii* (see Tables 1–2 in S1 Dataset for study design). Principal component analysis showed that co-infection, while positioned close to mono-infection,

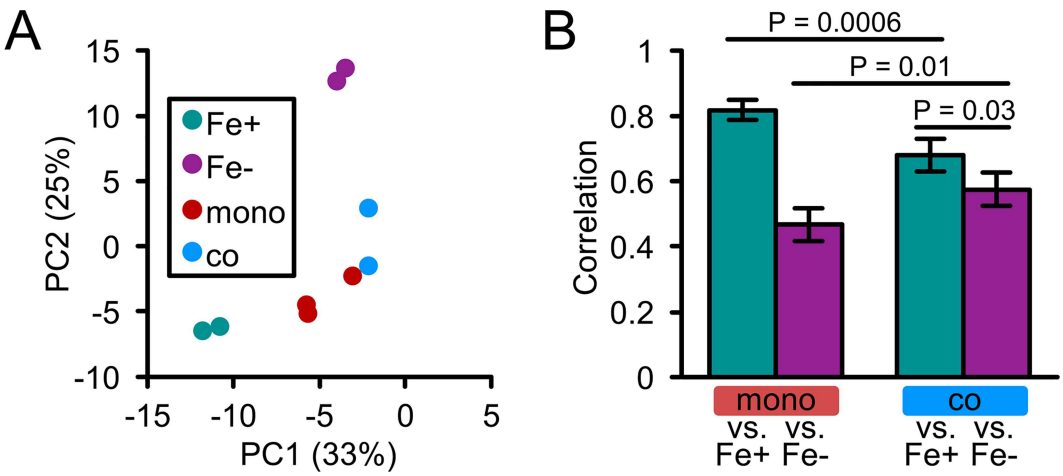

Fig 6. *A. actinomycetemcomitans* is iron-restricted in murine abscess co-infection. (A) Principal component analysis of the 93 genes regulated by iron. Each dot is a single replicate. Legend: Fe+, biofilm on rich media; Fe-, biofilm on iron-chelated media; mono, abscess mono-infection; co, abscess co-infection with *S. gordonii*. Axes: Percentages are the amount of variation captured by each principal component. (B) Correlation analysis of the 93 genes regulated by iron. Spearman's rank correlation was determined by comparing Fe+ and Fe- *in vitro* biofilms to *A. actinomycetemcomitans* gene expression in mono-infection (mono vs. Fe+ and Fe-) or co-infection with *S. gordonii* (co vs. Fe+ and Fe-). Error bars represent standard deviation (n = 4–6 pairwise comparisons). Significance was determined using a 2-tailed t test.

doi:10.1371/journal.ppat.1006084.g006

shifts the abscess towards Fe- biofilms (Fig 6A). Furthermore, the correlation between co-infection and Fe- biofilms was higher than that between mono-infection and Fe- biofilms (Fig 6B). In addition, genes upregulated in response to *S. gordonii* were enriched for genes upregulated by iron restriction (Table 7 in S1 Dataset) including 5 involved in iron uptake (S2 Dataset). Together, these results indicate that *A. actinomycetemcomitans* is restricted for iron during co-infection with *S. gordonii*.

How is iron restricted in co-infected abscesses? One possible mechanism for this interaction is direct interspecies competition for iron, as this has been reported in other mixed-species infections [18]. However, *S. gordonii* and other streptococci do not have an absolute growth requirement for iron [61], suggesting that interspecies competition is likely not responsible for reducing iron availability in co-infection. Supporting this, we found little evidence that *S. gordonii* differentially expresses genes related to iron homeostasis in either mono- or co-infection (Table 8 in S1 Dataset, S4 Dataset). Based on these data, we hypothesize that reduced iron in co-infection results from increased *A. actinomycetemcomitans* intraspecies competition (S5B Fig), a result of the 5–10 fold higher *A. actinomycetemcomitans* cell numbers observed during co-infection [39, 54, 62]. This higher bacterial burden could also enhance the host immune response and sequestration of iron within the abscess.

Since iron restriction induces *dspB* expression (Fig 1), a possible implication of the iron restriction associated with co-infection is that *A. actinomycetemcomitans* spatially reorganizes in response to *S. gordonii*. Previously we showed that *A. actinomycetemcomitans* proliferates in the abscess as small groups of cells (aggregates) and that the size of these aggregates is controlled by *dspB* [54]. Therefore, we anticipate that since *S. gordonii* restricts iron, *A. actinomycetemcomitans* forms smaller aggregates in co-infection than mono-infection. Of note, this spatial reorganization could facilitate iron acquisition since theoretically more cells per aggregate, due to the higher surface area to volume ratio, would have access to iron (S5C Fig). Current studies in our lab are aimed at addressing these possibilities.

The *A. actinomycetemcomitans* iron and Fur regulons in human periodontitis

Our abscess model provided a relatively simple *in vivo* environment for investigating the role of iron in interactions between *A. actinomycetemcomitans*, the host, and a co-infecting bacterium. To investigate the role of iron in a more complex polymicrobial environment, we next analyzed expression of the *A. actinomycetemcomitans* iron and Fur regulons during human periodontal disease. To do this, we extracted sequencing reads mapping to *A. actinomycetemcomitans* from a published meta-transcriptomics dataset comparing microbial gene expression from paired healthy and diseased (periodontitis) sites in the human oral cavity [63] (see Tables 1–2 in S1 Dataset for study design). Using principal component and correlation analyses, we showed that *A. actinomycetemcomitans* from healthy communities lies closer to Fe+ than Fe- biofilms (Fig 7A), but correlates to the same extent with both conditions (Fig 7B). In contrast, *A. actinomycetemcomitans* from diseased communities was closer to (Fig 7A) and correlated better with Fe- than Fe+ biofilms (Fig 7B). We obtained similar results for the Fur regulon (S3 Fig), specifically that disease was closer than health to the *Δfur* mutant. Furthermore, genes upregulated in periodontitis were enriched for both genes upregulated by iron restriction and repressed by Fur (Table 9 in S1 Dataset). These included several transporters for various iron sources. Notably, 3 of the 5 genes coding for the ferrous iron transporter were upregulated in periodontitis (S2 Dataset). This suggests that ferrous iron is an important iron source for *A. actinomycetemcomitans* in periodontal disease. We also found that the first gene in the *dspB* operon is upregulated in periodontitis. As DspB is stimulated not only by low iron (Fig 3) but also oxygen [54], we propose a model where *A. actinomycetemcomitans* disperses and migrates to deeper, anaerobic niches of the gingival pocket [21] during disease. As to why iron is restricted at diseased compared to healthy oral sites, we suspect that this phenomenon stems from a combination of the heightened host immune response (potentially resulting in greater iron sequestration) and the higher bacterial burden (potentially resulting in greater interspecies competition for iron) (S5D Fig).

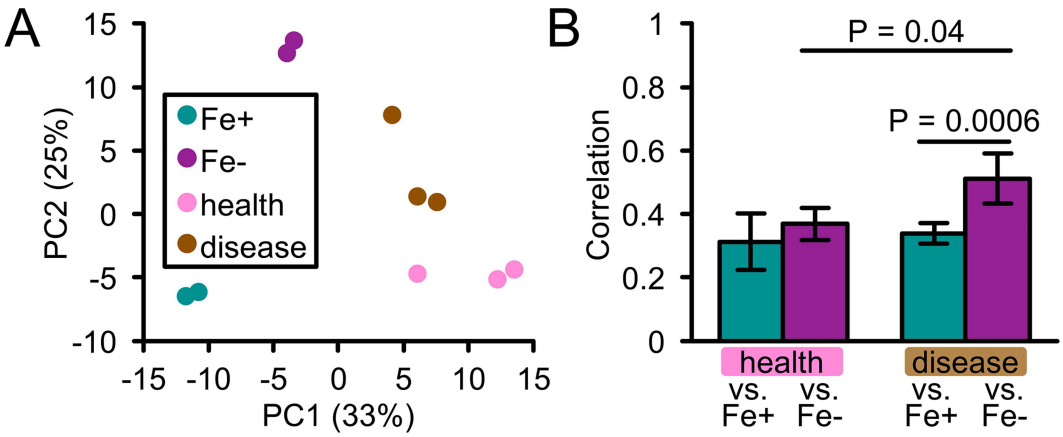

Fig 7. *A. actinomycetemcomitans* is iron-restricted in human periodontitis. (A) Principal component analysis of the 93 genes regulated by iron. Legend: Fe+, biofilm on rich media; Fe-, biofilm on iron-chelated media; health, *A. actinomycetemcomitans* from healthy human gingival crevice; disease, *A. actinomycetemcomitans* from diseased human gingival crevice. Axes: Percentages are the amount of variation captured by each principal component. (B) Correlation analysis of the 93 genes regulated by iron. Spearman's rank correlation was determined by comparing Fe+ and Fe- *in vitro* biofilms to *A. actinomycetemcomitans* gene expression in healthy human gingival crevice samples (health vs. Fe+ and Fe-) or diseased human gingival crevice samples (disease vs. Fe+ and Fe-). Error bars represent standard deviation (n = 6 pairwise comparisons). Significance was determined using a 2-tailed t test.

doi:10.1371/journal.ppat.1006084.g007

Conclusions

In summary, our *in vitro* analysis of the iron-restricted and Fur regulons of *A. actinomycetemcomitans* allowed us to gauge its behavior regarding iron levels in multiple infection sites. We discovered that Fur has a complex role, impacting not only *A. actinomycetemcomitans* iron homeostasis but also biofilm dispersal. Our observation that *A. actinomycetemcomitans* disperses from biofilms in iron-restricted environments suggests that this pathogen may overcome host iron restriction via actively promoting spatial re-localization. Of additional interest, we also found that the availability of iron to *A. actinomycetemcomitans* is heterogeneous *in vivo*. Indeed, while iron does not appear to be restricted in *A. actinomycetemcomitans* monospecies abscess infections, co-culture abscess infections and human gum disease appear to be iron-restricted infections. Collectively these results suggest that microbial pathogens use multiple methods (iron acquisition and spatial re-localization) to acquire iron during infection, and that co-infecting bacteria have a significant impact on whether a pathogen is restricted for iron.

Materials and Methods

Ethics statement

This study was performed in accordance with recommendations in the Guide for the Care and Use of Laboratory Animals of the National Institutes of Health. The animal protocol was approved by the Institutional Animal Care and Use Committee of The University of Texas at Austin (protocol number 00136). Mice were anesthetized with isoflurane delivered from a precision vaporizer and euthanized by asphyxiation with CO_2 followed by cervical dislocation.

Strains and growth conditions

A. actinomycetemcomitans 624 (a clinical isolate), *A. actinomycetemcomitans* VT1169 (a laboratory strain [64]) and *Streptococcus gordonii* Challis DL1.1 (ATCC 49818) were used in this study. Cultures were routinely grown in tryptic soy broth/agar (BD Difco) supplemented with 0.5% (w/vol) yeast extract (Fluka) (broth, TSBYE; agar, TSAYE) in a 5% CO_2 atmosphere with shaking at 250 rpm for *A. actinomycetemcomitans*. Anaerobic cultures were grown in a vinyl chamber (Coy) supplied with the following gas mixture: 85% N_2, 10% CO_2, 5% H_2. Colony biofilms were formed by spotting 100 μl of culture (adjusted to OD_{600} = 1) onto a polycarbonate, 0.2 μm pore size membrane (Whatman) placed onto the surface of a TSAYE plate.

Strain construction

The *A. actinomycetemcomitans* 624 *Δfur* mutant was constructed by replacing the *fur* gene with a gene encoding spectinomycin resistance (*aad9*) by natural transformation as previously described [54] (see S2 Table for primer sequences). To construct the *A. actinomycetemcomitans* 624 strain for ChIP-seq, the *fur* gene and promoter region (~500 bp upstream of the *fur* start codon) were PCR-amplified from *A. actinomycetemcomitans* 624 genomic DNA with primers fur-pro-1-F and fur-tag-1-R, the reverse primer being designed to insert the VSV-G tag directly in front of the *fur* stop codon. This PCR product was then ligated into the TA vector pGEM-T Easy (Promega) and TSS transformed [65] into *E. coli* DH5α. A plasmid with the insert was then purified and used as the template for a second PCR with primers fur-pro-2-F and fur-tag-2-R, designed to incorporate KpnI restriction sites at the ends of the insert. Like the first PCR product, the second PCR product was cloned into pGEM-T Easy (Promega) and TSS transformed [65] into *E. coli* DH5α. A plasmid with the insert was then purified, digested with KpnI, and the VSV-G tagged *fur* gene was purified by gel extraction. The target vector

pYGK [66] was also digested with KpnI, dephosphorylated with calf intestinal alkaline phosphatase (CIP), and purified. The KpnI-digested VSV-G tagged *fur* gene was then ligated into KpnI-digested, CIP-treated pYGK and TSS transformed into DH5α. This final plasmid was purified and electroporated as described [67] into the *A. actinomycetemcomitans* 624 *Δfur* mutant to generate the ChIP-seq strain. Plasmid inserts were sequenced at the UT Austin DNA Sequencing Facility.

RNA-seq

Colony biofilms of the *A. actinomycetemcomitans* 624 wild type and *Δfur* mutant were prepared and grown overnight under anaerobic conditions. Biofilms were then transferred to fresh locations on the same plate, incubated for 2 hours, and then transferred to new plates, either TSAYE (+Fe condition) or TSAYE + 250 μM 2,2'-dipyridyl (-Fe condition). (This concentration of 2,2'-dipyridyl reduces the growth rate and yield of planktonic *A. actinomycetemcomitans* by approximately 50% [25], and fully restricts the growth of *A. actinomycetemcomitans* iron transport mutants on streak plates [27].) Biofilms were then further incubated for 2 hours, and following this they were stored in RNAlater solution. Per replicate, 8 colony biofilms were pooled together for each treatment (+Fe wild type, -Fe wild type, +Fe *Δfur*, -Fe *Δfur*), and altogether 2 replicates were performed, each on different days (Table 1 in S1 Dataset). Biofilm RNA was extracted with RNA-Bee (Tel-Test) according to the manufacturer's protocol. Abscess RNA was extracted as previously described [58] from 1 or 2 pooled abscesses per biological replicate. Extracted RNA was treated with RQ1 DNase (Promega) to remove DNA contamination, and DNA removal was verified by PCR of the *clpX* gene. RNA integrity was verified by agarose gel separation of RNA denatured with NorthernMax-Gly loading dye (Ambion). Bacterial rRNA depletion, RNA fragmentation, and RNA-seq library preparation were performed as previously described [68], except that co-infected abscess RNA-seq libraries were rRNA-depleted with the MICROBEnrich and MICROBExpress kits (Ambion) and size-selected for fragments between 130–200 bp. Libraries were sequenced on 1x100 single-end Illumina HiSeq runs at the UT Austin Genome Sequencing and Analysis Facility. RNA-seq data were deposited into the NCBI Sequence Read Archive under accessions SRP081045 and SRP093165.

ChIP-seq

Colony biofilms of *A. actinomycetemcomitans* 624 *Δfur* expressing VSV-G tagged *fur* were prepared and treated as described for the RNA-seq experiment, with the exception that growth plates included 10 μg/ml kanamycin to maintain the ChIP-seq plasmid. After 2 h incubation in the +Fe and -Fe conditions, biofilms were placed into 50 ml TSBYE + 1% formaldehyde per treatment, gently agitated for 20 min at room temperature, and then vigorously vortexed to dislodge the cells from the membranes. For abscess infections, the *A. actinomycetemcomitans* 624 *Δfur* strain expressing VSV-G tagged *fur* was first grown overnight in TSBYE + 10 μg/ml kanamycin under anaerobic conditions. Then, 3 ml of culture were washed and resuspended in 1 ml TSBYE, and 100 μl were injected into each thigh of three 10-week-old mice to form abscesses [62]. After 3 days, abscesses were harvested and each placed into 1 ml TSBYE + 5% formaldehyde. After overnight fixation, abscesses were homogenized, and the homogenates were collected by centrifugation and washed with TSBYE. Eight biofilms and 3 abscesses were used per experiment, and experiments were performed twice. At this point, the fixed biofilm cells and fixed abscess homogenates were subjected to the same ChIP procedure [37]. First, fixed samples were added with 0.5 M glycine to quench crosslinking. Samples were then washed with TBS (50 mM Tris-HCl, pH 7.5; 150 mM NaCl), each resuspended in 1 ml lysis

buffer (10 mM Tris-HCl, pH 8; 100 mM NaCl; 1 mM EDTA; 0.5 mM EGTA; 0.1% deoxycholate; 0.5% N-lauroylsarcosine) + 1 mg/ml lysozyme + protease inhibitor (Sigma), and incubated at 37˚C for 30 min. The samples were then chilled on ice, sonicated 2x for 5 s, or until the solution became clear, with a tip sonicator (QSonica) at 60% amplitude, and then further sonicated at 4˚C for 20 min in 10 s on/10 s off cycles with a Q800R sonicator (QSonica) at 60% amplitude. Lysates were then separated from unlysed debris by centrifugation, and 25 μl of each clarified lysate was saved for the ChIP input control. A 1/10 volume of Triton X-100 (10% solution in lysis buffer) was then added to each sample, followed by 25 μl of Protein G Dynabeads (ThermoFisher) coated with anti-VSV-G monoclonal antibody (Sigma). The samples were rotated overnight at 4˚C, and following this, each sample was washed 5x with 1 ml RIPA buffer (50 mM HEPES, pH 7.5; 500 mM LiCl; 1 mM EDTA; 1% Nonidet P-40; 0.7% deoxycholate), 1x with 1 ml TE (10 mM Tris-HCl, pH 8; 1 mM EDTA) + 50 mM NaCl, and resuspended in 100 μl EB (50 mM Tris-HCl, pH 7.5; 10 mM EDTA; 1% SDS). The samples were then incubated at 65˚C for 30 min, separated from the Dynabeads by centrifugation, and further incubated overnight, along with the ChIP inputs, at 65˚C to reverse crosslinks. Following this, the samples were brought up to 200 μl in volume with TE, incubated with 8 μl 10 mg/ml RNase A for 2 h at 37˚C, and further incubated with 4 μl 20 mg/ml proteinase K for 2 h at 55˚C. Finally, samples were purified with the ChIP DNA Clean & Concentrator kit (Zymo Research), and ChIP-seq libraries were prepared using the NEBNext ChIP-Seq Library Master Mix Set according to the manufacturer's instructions. Libraries were sequenced on 1x75 single-end Illumina NextSeq runs at the UT Austin Genome Sequencing and Analysis Facility. ChIP-seq data were deposited into the NCBI Sequence Read Archive under accession SRP081045.

Genome sequencing

A. actinomycetemcomitans 624 genome sequencing and assembly were performed as previously described [62]. Annotation was performed with PGAP [69], RAST [70], and KAAS [71]. Noncoding RNA sequences [58] were extracted from the D7S-1 genome with the bedtools getfasta function [72] and mapped to the *A. actinomycetemcomitans* 624 genome with bowtie2 v2.2.5 in very-sensitive-local mode [73]. Raw genome sequences were deposited into the NCBI Sequence Read Archive under accession SRP064936. The genome assembly was deposited into GenBank under accession CP012959.

RNA-seq analysis

Raw reads were processed with cutadapt v1.9.1 (and higher) (http://cutadapt.readthedocs.org/en/stable/index.html) to (1) trim 3' low-quality bases (cutoff: 15), (2) trim 3' adaptors (sequence: AGATCGGAAGAGCACACGTCTGAACTCCAGTCAC), and (3) discard short reads (minimum length: 10 bases for non-human samples, or 15 bases for human samples,). Processed reads were mapped to the *A. actinomycetemcomitans* 624 or *S. gordonii* genome with bowtie2 v2.2.5 in very-sensitive-local mode [73], and only reads with mapping quality (MAPQ) scores $\geq$39 for non-human samples, or $\geq$20 for human samples, were kept for further analysis. Reads were counted per gene strand-specifically with the featureCounts function in Rsubread v1.20 (and higher) [74]. Raw read counts, excluding rRNA and tRNA, were adjusted for between-sample differences in sequencing depth with the estimateSizeFactors function in DESeq2 v1.10.1 (and higher) [75]. Raw read counts were also normalized for between-gene differences in GC content by including a normalization matrix. This normalization matrix was generated with the withinLaneNormalization function in EDASeq v2.4.1 (and higher) [76], and transformed to be on the scale of read counts, as described in the DESeq2 vignette. GC content values for the matrix were calculated with the nucBed function in

bedtools v2.20 (and higher) [72]. Default DESeq2 parameters were used for estimating dispersions and performing the Wald test for differential expression analysis, and a multi-factor design, as described in the DESeq2 vignette, was used for paired analysis of healthy and diseased human from each patient [63]. Significance cutoffs were as follows. Iron-restricted, Fur, and co-infection regulons: $\log_2$ fold change (FC) > 0.5; adjusted P value < 0.05. Periodontitis: $\log_2$ FC > 0.5; non-adjusted P < 0.05. See Table 10 in S1 Dataset for a summary of the RNA-seq data analysis. Analyses were performed both locally and on the UT Austin Texas Advanced Computer Center.

ChIP-seq analysis

Raw reads were processed as described for the RNA-seq analysis. Binding regions (peaks) were called with MOSAiCS v2.9.9 [77]. Adjustable MOSAiCS parameters were: fragLen, 200; binSize, 50; capping, 3; bgEst, automatic; FDR, 0.1. The control for colony biofilm samples was the *in vitro* ChIP input, and the control for abscess samples was the *in vivo* ChIP input. Promoters were defined for coding genes as the 200 and 50 bp up- and downstream of the start codon and for noncoding genes as the 100 and 25 bp up- and downstream of the start codon. The number of peaks overlapping each promoter was counted for each sample with the bedtools intersectBed function [72]. Peaks were only counted if they overlapped at minimum 50 bp of coding promoters or 25 bp of noncoding promoters. After tallying overlapping peaks, promoters were only considered bound by Fur if they overlapped a peak in at least 2 *in vitro* biofilm replicates. If one of these promoters also overlapped a peak in at least 1 of the abscess replicates, it was considered also bound by Fur *in vivo*. Promoters overlapping peaks in both Fe+ biofilm replicates were considered preferentially bound in the presence of iron, and promoters overlapping peaks in both Fe- biofilm replicates were considered preferentially bound in the absence of iron. See Tables 11–12 in S1 Dataset for a summary of the ChIP-seq data analysis. Analyses were performed both locally and on the UT Austin Texas Advanced Computer Center.

Binding motif analysis

Promoter sequences were extracted from the *A. actinomycetemcomitans* 624 genome with the bedtools getfasta function [72] and submitted to MEME [78] to identify consensus binding motifs. MEME settings were: site distribution, zero or one occurrence per sequence; background model, 0-order model of sequences; minimum motif width, 15; maximum motif width, 25. A CRP box was identified among the promoters of genes activated by Fur, and a Fur box was identified among the promoters directly bound by Fur. Each binding motif was submitted to the MEME Suite program FIMO [78] to calculate the significance (FDR) of its occurrence within each promoter of its respective promoter set.

sRNA target prediction

sRNA sequences were extracted from the *A. actinomycetemcomitans* 624 genome with the bedtools getfasta function [72] and submitted to TargetRNA2 [43] with default parameters and the *A. actinomycetemcomitans* strain D7S-1 genome selected. Predicted target sequences in the D7S-1 genome were mapped in fasta format to the *A. actinomycetemcomitans* 624 genome with bowtie2 v2.2.5 in very-sensitive-local mode [73].

CRP regulon

The *A. actinomycetemcomitans* CRP regulon was determined with a microarray designed for strain HK1651 [46]. To use this data, *A. actinomycetemcomitans* 624 gene sequences in fasta

format were mapped to the *A. actinomycetemcomitans* HK1651 genome with bowtie2 v2.2.5 in very-sensitive-local mode [73].

Principal component analysis

Normalized read counts were transformed with the DESeq2 [75] rlog method with blindness set to false, as described in the DESeq2 vignette, and the PCA was performed with the prcomp function in R on the 93 genes in the iron-restricted regulon or the 218 genes in the Fur regulon.

β-galactosidase assay

β-galactosidase assays were performed as previously described [54] using a chemiluminescent assay system (Galacto-Light Plus).

Biofilm dispersal assay

The biofilm dispersal assay was performed as previously described [54].

Abscess model

The murine abscess infection model was performed as previously described [39, 62], except that in the experiment testing the virulence of the *Δfur* mutant, anaerobic conditions were used for preparing the inoculum and plating serial dilutions of the abscess homogenates.

Accession numbers

All RNA-seq and ChIP-seq files are available from the National Center for Biotechnology Information Sequence Read Archive (accession numbers SRP081045 and SRP093165).

Supporting Information

S1 Fig. Scatter plots of the *A. actinomycetemcomitans* iron-restricted and Fur regulons. (A) Genes differentially expressed in response to iron restriction. Y axis: fold change (FC) comparing iron-chelated to rich media. Legend: blue dots represent genes differentially expressed >4 fold comparing iron-chelated to rich media. (B) Genes differentially expressed in the *Δfur* mutant. Y axis: Fold change (FC) comparing the *Δfur* mutant to the wild type (wt). Left: comparison on rich media. Right: comparison on iron-chelated media. Legend: red dots represent genes that are regulated by both Fur and iron. (C) Genes whose promoters are bound by Fur. Rows: ChIP, all Fur-bound promoters; low Fe, Fur-bound promoters of genes differentially expressed in response to iron restriction; *Δfur*, Fur-bound promoters of genes differentially expressed in the *Δfur* mutant.
(TIF)

S2 Fig. Indirect regulation in *A. actinomycetemcomitans Δfur*. (A) Transcriptional regulators differentially expressed in the *Δfur* mutant. The cellular process controlled by each regulator is indicated in parentheses. Colors: purple, repressed by Fur; green, activated by Fur. (B) A CRP binding motif was found with False Discovery Rate < 0.1 in 64 of the 218 promoters of Fur activated genes.
(TIF)

S3 Fig. The *A. actinomycetemcomitans* Fur regulon *in vivo*. (A) Principal component analysis of the 218 genes differentially expressed in the *Δfur* mutant. Each dot is a single replicate. Legend: wt, wild-type biofilm on rich media; *Δfur*, *Δfur* biofilm on rich media; mono, abscess

mono-infection; co, abscess co-infection with *S. gordonii*; health, *A. actinomycetemcomitans* from healthy human gingival crevice; disease, *A. actinomycetemcomitans* from diseased human gingival crevice. Axes: Percentages are the amount of variation captured by each principal component. (B) Correlation analysis of the 218 genes differentially expressed in the *Δfur* mutant. Spearman's rank correlation was determined by comparing Fe+ and Fe- *in vitro* biofilms to *A. actinomycetemcomitans* gene expression in mono-infection (mono vs. Fe+ and Fe-), co-infection with *S. gordonii* (co vs. Fe+ and Fe-), healthy human gingival crevice samples (health vs. Fe+ and Fe-), or diseased human gingival crevice samples (disease vs. Fe+ and Fe-). Error bars represent standard deviation (n = 4–6 pairwise comparisons). Significance was determined using a 2-tailed t test ([a], unpaired test; [b], paired test).
(TIF)

S4 Fig. Cellular processes differentially expressed in periodontitis. Each shown process is encoded by a gene(s) that is regulated by iron restriction and/or Fur. Q, quinone; R, respiratory reductase; AI-2, autoinducer-2; GAP, glyceraldehyde-3P; Ac-CoA, acetyl-CoA; UMP, uridine monophosphate; 2+ in circle, free ferrous iron; 3+ in circle, free ferric iron; 3+ in square, ferric iron siderophore; Ala, alanine; Gly, glycine; hairpin, sRNA.
(TIF)

S5 Fig. Model for iron dynamics in *A. actinomycetemcomitans* abscess and oral cavity infections. (A) Iron in mono-infected abscesses may be high (left) (e.g. if the host were not to fully sequester iron), low (middle), or low but spatially uneven (right), forming concentrated patches. These patches could induce *A. actinomycetemcomitans* to grow as aggregates. (B) *A. actinomycetemcomitans* in mono-infected abscesses (*Aa*, left) is not restricted for iron, but in co-infected abscesses with *S. gordonii* (*Aa* + *Sg*, right), higher *A. actinomycetemcomitans* titers may result in greater competition over iron between cells of *A. actinomycetemcomitans*. (C) In mono-infection (*Aa*, left), cells at the center of aggregates may not be restricted for iron, but in co-infection prior to dispersal (*Aa* + *Sg* pre-disp, middle), reduced iron may prevent these cells' access to iron. Therefore, the formation of smaller aggregates after dispersal (*Aa* + *Sg* post-disp) may restore cellular access to iron. (D) The host immune response and higher bacterial burden associated with periodontitis (right) may create a larger iron gradient than seen in health (left), inducing *A. actinomycetemcomitans* to spread deeper into the gingival crevice (space between tooth and gum).
(TIF)

S1 Dataset.
(DOCX)

S2 Dataset.
(XLSX)

S3 Dataset.
(XLSX)

S4 Dataset.
(XLSX)

S1 Table.
(DOCX)

S2 Table.
(DOCX)

Acknowledgments

We thank Dr. Bryan Davies for assistance with the ChIP procedure, Dr. Daniel Cornforth for assistance with assembling the *A. actinomycetemcomitans* 624 genome, and Dr. Kendra Rumbaugh for assistance with the abscess infections.

Author Contributions

Conceptualization: AS MW.

Data curation: AS.

Formal analysis: AS.

Funding acquisition: AS MW.

Investigation: AS NA PJ.

Methodology: AS NA PJ MW.

Project administration: MW.

Resources: AS MW.

Software: AS.

Supervision: MW.

Validation: AS MW.

Visualization: AS.

Writing – original draft: AS.

Writing – review & editing: AS MW.

References

1. Schade AL, Caroline L. Raw hen egg white and the role of iron in growth inhibition of *Shigella dysenteriae*, *Staphylococcus aureus*, *Escherichia coli* and *Saccharomyces cerevisiae*. Science. 1944; 100 (2584):14–5. doi: 10.1126/science.100.2584.14 PMID: 17783793
2. Weinberg ED. Role of iron in host-parasite interactions. J Infect Dis. 1971; 124(4):401–10. PMID: 4947218
3. Bullen JJ. The significance of iron in infection. Rev Infect Dis. 1981; 3(6):1127–38. PMID: 7043704
4. Weinberg ED. Iron and susceptibility to infectious disease. Science. 1974; 184(4140):952–6. PMID: 4596821
5. Hood MI, Skaar EP. Nutritional immunity: transition metals at the pathogen-host interface. Nat Rev Microbiol. 2012; 10(8):525–37. PubMed Central PMCID: PMCPMC3875331. doi: 10.1038/nrmicro2836 PMID: 22796883
6. Barber MF, Elde NC. Buried treasure: evolutionary perspectives on microbial iron piracy. Trends Genet. 2015; 31(11):627–36. PubMed Central PMCID: PMCPMC4639441. doi: 10.1016/j.tig.2015.09.001 PMID: 26431675
7. Ganz T, Nemeth E. Iron homeostasis in host defence and inflammation. Nat Rev Immunol. 2015; 15 (8):500–10. PubMed Central PMCID: PMCPMC4801113. doi: 10.1038/nri3863 PMID: 26160612
8. Hem JD. Chemical Factors That Influence the Availability of Iron and Manganese in Aqueous Systems. Geological Society of America Special Papers. 1972; 140:17–24.
9. Ratledge C, Dover LG. Iron metabolism in pathogenic bacteria. Annu Rev Microbiol. 2000; 54:881–941. doi: 10.1146/annurev.micro.54.1.881 PMID: 11018148
10. Becker KW, Skaar EP. Metal limitation and toxicity at the interface between host and pathogen. FEMS Microbiol Rev. 2014; 38(6):1235–49. PubMed Central PMCID: PMCPMC4227937. doi: 10.1111/1574-6976.12087 PMID: 25211180

11. Carpenter BM, Whitmire JM, Merrell DS. This is not your mother's repressor: the complex role of *fur* in pathogenesis. Infect Immun. 2009; 77(7):2590–601. PubMed Central PMCID: PMCPMC2708581. doi: 10.1128/IAI.00116-09 PMID: 19364842

12. Mashburn LM, Jett AM, Akins DR, Whiteley M. *Staphylococcus aureus* serves as an iron source for *Pseudomonas aeruginosa* during *in vivo* coculture. J Bacteriol. 2005; 187(2):554–66. PubMed Central PMCID: PMCPMC543556. doi: 10.1128/JB.187.2.554-566.2005 PMID: 15629927

13. Deriu E, Liu JZ, Pezeshki M, Edwards RA, Ochoa RJ, Contreras H, et al. Probiotic bacteria reduce *Salmonella* Typhimurium intestinal colonization by competing for iron. Cell Host Microbe. 2013; 14(1):26–37. PubMed Central PMCID: PMCPMC3752295. doi: 10.1016/j.chom.2013.06.007 PMID: 23870311

14. Hendricks MR, Lashua LP, Fischer DK, Flitter BA, Eichinger KM, Durbin JE, et al. Respiratory syncytial virus infection enhances *Pseudomonas aeruginosa* biofilm growth through dysregulation of nutritional immunity. Proc Natl Acad Sci U S A. 2016; 113(6):1642–7. PubMed Central PMCID: PMCPMC4760822. doi: 10.1073/pnas.1516979113 PMID: 26729873

15. Otto BR, van Dooren SJ, Dozois CM, Luirink J, Oudega B. *Escherichia coli* hemoglobin protease autotransporter contributes to synergistic abscess formation and heme-dependent growth of *Bacteroides fragilis*. Infect Immun. 2002; 70(1):5–10. PubMed Central PMCID: PMCPMC127594. doi: 10.1128/IAI.70.1.5-10.2002 PMID: 11748157

16. Keogh D, Tay WH, Ho YY, Dale JL, Chen S, Umashankar S, et al. Enterococcal metabolite cues facilitate interspecies niche modulation and polymicrobial infection. Cell Host Microbe. 2016; 20(4):493–503. PubMed Central PMCID: PMCPMC5076562. doi: 10.1016/j.chom.2016.09.004 PMID: 27736645

17. Fine DH, Furgang D, Beydouin F. Lactoferrin iron levels are reduced in saliva of patients with localized aggressive periodontitis. J Periodontol. 2002; 73(6):624–30. doi: 10.1902/jop.2002.73.6.624 PMID: 12083535

18. Jordan WJ, Eskdale J, Lennon GP, Pestoff R, Wu L, Fine DH, et al. A non-conservative, coding single-nucleotide polymorphism in the N-terminal region of lactoferrin is associated with aggressive periodontitis in an African-American, but not a Caucasian population. Genes Immun. 2005; 6(7):632–5. doi: 10.1038/sj.gene.6364239 PMID: 16208406

19. Hutter JW, van der Velden U, Varoufaki A, Huffels RA, Hoek FJ, Loos BG. Lower numbers of erythrocytes and lower levels of hemoglobin in periodontitis patients compared to control subjects. J Clin Periodontol. 2001; 28(10):930–6. PMID: 11686811

20. Darveau RP. Periodontitis: a polymicrobial disruption of host homeostasis. Nat Rev Microbiol. 2010; 8(7):481–90. doi: 10.1038/nrmicro2337 PMID: 20514045

21. Loesche WJ, Gusberti F, Mettraux G, Higgins T, Syed S. Relationship between oxygen tension and subgingival bacterial flora in untreated human periodontal pockets. Infect Immun. 1983; 42(2):659–67. PubMed Central PMCID: PMCPMC264480. PMID: 6642647

22. Mukherjee S. The role of crevicular fluid iron in periodontal disease. J Periodontol. 1985; 56(11 Suppl):22–7. doi: 10.1902/jop.1985.56.11s.22 PMID: 3908636

23. Duran-Pinedo AE, Chen T, Teles R, Starr JR, Wang X, Krishnan K, et al. Community-wide transcriptome of the oral microbiome in subjects with and without periodontitis. ISME J. 2014; 8(8):1659–72. PubMed Central PMCID: PMCPMC4817619. doi: 10.1038/ismej.2014.23 PMID: 24599074

24. Zambon JJ. *Actinobacillus actinomycetemcomitans* in human periodontal disease. J Clin Periodontol. 1985; 12(1):1–20. PMID: 3882766

25. Winston JL, Chen CK, Neiders ME, Dyer DW. Membrane protein expression by *Actinobacillus actinomycetemcomitans* in response to iron availability. J Dent Res. 1993; 72(10):1366–73. PMID: 8408878

26. Hayashida H, Poulsen K, Kilian M. Differences in iron acquisition from human haemoglobin among strains of *Actinobacillus actinomycetemcomitans*. Microbiology. 2002; 148(Pt 12):3993–4001. doi: 10.1099/00221287-148-12-3993 PMID: 12480903

27. Rhodes ER, Menke S, Shoemaker C, Tomaras AP, McGillivary G, Actis LA. Iron acquisition in the dental pathogen *Actinobacillus actinomycetemcomitans*: what does it use as a source and how does it get this essential metal? Biometals. 2007; 20(3–4):365–77. doi: 10.1007/s10534-006-9058-3 PMID: 17206384

28. Mukherjee S, Murphy RA, Wawszkiewcz EJ. Effect of hemoglobin and of ferric ammonium citrate on the virulence of periodontopathic bacteria. Oral Microbiol Immunol. 1988; 3(4):192–5. PMID: 3254476

29. Velusamy SK, Poojary R, Ardeshna R, Alabdulmohsen W, Fine DH, Velliyagounder K. Protective effects of human lactoferrin during *Aggregatibacter actinomycetemcomitans*-induced bacteremia in lactoferrin-deficient mice. Antimicrob Agents Chemother. 2014; 58(1):397–404. PubMed Central PMCID: PMCPMC3910771. doi: 10.1128/AAC.00020-13 PMID: 24189260

30. Haraszthy VI, Jordan SF, Zambon JJ. Identification of Fur-regulated genes in *Actinobacillus actinomycetemcomitans*. Microbiology. 2006; 152(Pt 3):787–96. doi: 10.1099/mic.0.28366-0 PMID: 16514158

31. Hayashi M, Nakayama Y, Unemoto T. Existence of Na+-translocating NADH-quinone reductase in *Haemophilus influenzae*. FEBS Lett. 1996; 381(3):174–6. PMID: 8601449

32. Wissenbach U, Kroger A, Unden G. The specific functions of menaquinone and demethylmenaquinone in anaerobic respiration with fumarate, dimethylsulfoxide, trimethylamine N-oxide and nitrate by *Escherichia coli*. Arch Microbiol. 1990; 154(1):60–6. PMID: 2204318

33. Yamada H, Takashima E, Konishi K. Molecular characterization of the membrane-bound quinol peroxidase functionally connected to the respiratory chain. FEBS J. 2007; 274(3):853–66. doi: 10.1111/j.1742-4658.2006.05637.x PMID: 17288564

34. Willemsen PT, Vulto I, Boxem M, de Graaff J. Characterization of a periplasmic protein involved in iron utilization of *Actinobacillus actinomycetemcomitans*. J Bacteriol. 1997; 179(15):4949–52. PubMed Central PMCID: PMCPMC179347. PMID: 9244288

35. Rhodes ER, Tomaras AP, McGillivary G, Connerly PL, Actis LA. Genetic and functional analyses of the *Actinobacillus actinomycetemcomitans* AfeABCD siderophore-independent iron acquisition system. Infect Immun. 2005; 73(6):3758–63. PubMed Central PMCID: PMCPMC1111845. doi: 10.1128/IAI.73.6.3758-3763.2005 PMID: 15908408

36. Braun V. Energy-coupled transport and signal transduction through the gram-negative outer membrane via TonB-ExbB-ExbD-dependent receptor proteins. FEMS Microbiol Rev. 1995; 16(4):295–307. PMID: 7654405

37. Davies BW, Bogard RW, Mekalanos JJ. Mapping the regulon of *Vibrio cholerae* ferric uptake regulator expands its known network of gene regulation. Proc Natl Acad Sci U S A. 2011; 108(30):12467–72. PubMed Central PMCID: PMCPMC3145737. doi: 10.1073/pnas.1107894108 PMID: 21750152

38. Pittman MS, Corker H, Wu G, Binet MB, Moir AJ, Poole RK. Cysteine is exported from the *Escherichia coli* cytoplasm by CydDC, an ATP-binding cassette-type transporter required for cytochrome assembly. J Biol Chem. 2002; 277(51):49841–9. doi: 10.1074/jbc.M205615200 PMID: 12393891

39. Ramsey MM, Rumbaugh KP, Whiteley M. Metabolite cross-feeding enhances virulence in a model polymicrobial infection. PLoS Pathog. 2011; 7(3):e1002012. PubMed Central PMCID: PMCPMC3069116. doi: 10.1371/journal.ppat.1002012 PMID: 21483753

40. Yeh JI, Chinte U, Du S. Structure of glycerol-3-phosphate dehydrogenase, an essential monotopic membrane enzyme involved in respiration and metabolism. Proc Natl Acad Sci U S A. 2008; 105(9):3280–5. PubMed Central PMCID: PMCPMC2265192. doi: 10.1073/pnas.0712331105 PMID: 18296637

41. Carmel-Harel O, Storz G. Roles of the glutathione- and thioredoxin-dependent reduction systems in the *Escherichia coli* and *Saccharomyces cerevisiae* responses to oxidative stress. Annu Rev Microbiol. 2000; 54:439–61. doi: 10.1146/annurev.micro.54.1.439 PMID: 11018134

42. Santana EA, Harrison A, Zhang X, Baker BD, Kelly BJ, White P, et al. HrrF is the Fur-regulated small RNA in nontypeable *Haemophilus influenzae*. PLoS One. 2014; 9(8):e105644. PubMed Central PMCID: PMCPMC4144887. doi: 10.1371/journal.pone.0105644 PMID: 25157846

43. Kery MB, Feldman M, Livny J, Tjaden B. TargetRNA2: identifying targets of small regulatory RNAs in bacteria. Nucleic Acids Res. 2014; 42(Web Server issue):W124–9. PubMed Central PMCID: PMCPMC4086111. doi: 10.1093/nar/gku317 PMID: 24753424

44. Campoy S, Jara M, Busquets N, de Rozas AM, Badiola I, Barbe J. Intracellular cyclic AMP concentration is decreased in *Salmonella* Typhimurium *fur* mutants. Microbiology. 2002; 148(Pt 4):1039–48. doi: 10.1099/00221287-148-4-1039 PMID: 11932449

45. Zhang Z, Gosset G, Barabote R, Gonzalez CS, Cuevas WA, Saier MH Jr. Functional interactions between the carbon and iron utilization regulators, Crp and Fur, in *Escherichia coli*. J Bacteriol. 2005; 187(3):980–90. PubMed Central PMCID: PMCPMC545712. doi: 10.1128/JB.187.3.980-990.2005 PMID: 15659676

46. Feuerbacher LA, Burgum A, Kolodrubetz D. The cyclic-AMP receptor protein (CRP) regulon in *Aggregatibacter actinomycetemcomitans* includes leukotoxin. Microb Pathog. 2011; 51(3):133–41. PubMed Central PMCID: PMCPMC3120918. doi: 10.1016/j.micpath.2011.04.009 PMID: 21575705

47. Kanehisa M, Goto S, Sato Y, Kawashima M, Furumichi M, Tanabe M. Data, information, knowledge and principle: back to metabolism in KEGG. Nucleic Acids Res. 2014; 42(Database issue):D199–205. PubMed Central PMCID: PMCPMC3965122. doi: 10.1093/nar/gkt1076 PMID: 24214961

48. Friedman DB, Stauff DL, Pishchany G, Whitwell CW, Torres VJ, Skaar EP. *Staphylococcus aureus* redirects central metabolism to increase iron availability. PLoS Pathog. 2006; 2(8):e87. PubMed Central PMCID: PMCPMC1557832. doi: 10.1371/journal.ppat.0020087 PMID: 16933993

49. Torres-Escobar A, Juarez-Rodriguez MD, Lamont RJ, Demuth DR. Transcriptional regulation of *Aggregatibacter actinomycetemcomitans* IsrACDBFG and IsrRK operons and their role in biofilm formation. J Bacteriol. 2013; 195(1):56–65. PubMed Central PMCID: PMCPMC3536165. doi: 10.1128/JB.01476-12 PMID: 23104800

50. Balashova NV, Diaz R, Balashov SV, Crosby JA, Kachlany SC. Regulation of *Aggregatibacter* (*Actinobacillus*) *actinomycetemcomitans* leukotoxin secretion by iron. J Bacteriol. 2006; 188(24):8658–61. PubMed Central PMCID: PMCPMC1698250. doi: 10.1128/JB.01253-06 PMID: 17041062

51. Kachlany SC, Planet PJ, Bhattacharjee MK, Kollia E, DeSalle R, Fine DH, et al. Nonspecific adherence by *Actinobacillus actinomycetemcomitans* requires genes widespread in bacteria and archaea. J Bacteriol. 2000; 182(21):6169–76. PubMed Central PMCID: PMCPMC94753. PMID: 11029439

52. Mayer MP, Bueno LC, Hansen EJ, DiRienzo JM. Identification of a cytolethal distending toxin gene locus and features of a virulence-associated region in *Actinobacillus actinomycetemcomitans*. Infect Immun. 1999; 67(3):1227–37. PubMed Central PMCID: PMCPMC96451. PMID: 10024565

53. Kaplan JB, Velliyagounder K, Ragunath C, Rohde H, Mack D, Knobloch JK, et al. Genes involved in the synthesis and degradation of matrix polysaccharide in *Actinobacillus actinomycetemcomitans* and *Actinobacillus pleuropneumoniae* biofilms. J Bacteriol. 2004; 186(24):8213–20. PubMed Central PMCID: PMCPMC532409. doi: 10.1128/JB.186.24.8213-8220.2004 PMID: 15576769

54. Stacy A, Everett J, Jorth P, Trivedi U, Rumbaugh KP, Whiteley M. Bacterial fight-and-flight responses enhance virulence in a polymicrobial infection. Proc Natl Acad Sci U S A. 2014; 111(21):7819–24. PubMed Central PMCID: PMCPMC4040543. doi: 10.1073/pnas.1400586111 PMID: 24825893

55. Butcher J, Sarvan S, Brunzelle JS, Couture JF, Stintzi A. Structure and regulon of *Campylobacter jejuni* ferric uptake regulator Fur define apo-Fur regulation. Proc Natl Acad Sci U S A. 2012; 109(25):10047–52. PubMed Central PMCID: PMCPMC3382491. doi: 10.1073/pnas.1118321109 PMID: 22665794

56. Braun V, Hancock RE, Hantke K, Hartmann A. Functional organization of the outer membrane of *Escherichia coli*: phage and colicin receptors as components of iron uptake systems. J Supramol Struct. 1976; 5(1):37–58. doi: 10.1002/jss.400050105 PMID: 136550

57. Hammer ND, Skaar EP. Molecular mechanisms of *Staphylococcus aureus* iron acquisition. Annu Rev Microbiol. 2011; 65:129–47. PubMed Central PMCID: PMCPMC3807827. doi: 10.1146/annurev-micro-090110-102851 PMID: 21639791

58. Jorth P, Trivedi U, Rumbaugh K, Whiteley M. Probing bacterial metabolism during infection using high-resolution transcriptomics. J Bacteriol. 2013; 195(22):4991–8. PubMed Central PMCID: PMCPMC3811578. doi: 10.1128/JB.00875-13 PMID: 23974023

59. Stacy A, McNally L, Darch SE, Brown SP, Whiteley M. The biogeography of polymicrobial infection. Nat Rev Microbiol. 2016; 14(2):93–105. doi: 10.1038/nrmicro.2015.8 PMID: 26714431

60. Paster BJ, Olsen I, Aas JA, Dewhirst FE. The breadth of bacterial diversity in the human periodontal pocket and other oral sites. Periodontol 2000. 2006; 42:80–7. doi: 10.1111/j.1600-0757.2006.00174.x PMID: 16930307

61. Jakubovics NS, Jenkinson HF. Out of the iron age: new insights into the critical role of manganese homeostasis in bacteria. Microbiology. 2001; 147(Pt 7):1709–18. doi: 10.1099/00221287-147-7-1709 PMID: 11429449

62. Stacy A, Fleming D, Lamont RJ, Rumbaugh KP, Whiteley M. A commensal bacterium promotes virulence of an opportunistic pathogen via cross-respiration. MBio. 2016; 7(3). PubMed Central PMCID: PMCPMC4916382.

63. Jorth P, Turner KH, Gumus P, Nizam N, Buduneli N, Whiteley M. Metatranscriptomics of the human oral microbiome during health and disease. MBio. 2014; 5(2):e01012–14. PubMed Central PMCID: PMCPMC3977359. doi: 10.1128/mBio.01012-14 PMID: 24692635

64. Mintz KP. Identification of an extracellular matrix protein adhesin, EmaA, which mediates the adhesion of *Actinobacillus actinomycetemcomitans* to collagen. Microbiology. 2004; 150(Pt 8):2677–88. doi: 10.1099/mic.0.27110-0 PMID: 15289564

65. Chung CT, Niemela SL, Miller RH. One-step preparation of competent *Escherichia coli*: transformation and storage of bacterial cells in the same solution. Proc Natl Acad Sci U S A. 1989; 86(7):2172–5. PubMed Central PMCID: PMCPMC286873. PMID: 2648393

66. Brogan JM, Lally ET, Demuth DR. Construction of pYGK, an *Actinobacillus actinomycetemcomitans-Escherichia coli* shuttle vector. Gene. 1996; 169(1):141–2. PMID: 8635742

67. Sreenivasan PK, LeBlanc DJ, Lee LN, Fives-Taylor P. Transformation of *Actinobacillus actinomycetemcomitans* by electroporation, utilizing constructed shuttle plasmids. Infect Immun. 1991; 59(12):4621–7. PubMed Central PMCID: PMCPMC259087. PMID: 1937823

68. Turner KH, Everett J, Trivedi U, Rumbaugh KP, Whiteley M. Requirements for *Pseudomonas aeruginosa* acute burn and chronic surgical wound infection. PLoS Genet. 2014; 10(7):e1004518. PubMed Central PMCID: PMCPMC4109851. doi: 10.1371/journal.pgen.1004518 PMID: 25057820

69. Angiuoli SV, Gussman A, Klimke W, Cochrane G, Field D, Garrity G, et al. Toward an online repository of Standard Operating Procedures (SOPs) for (meta)genomic annotation. OMICS. 2008; 12(2):137–41. PubMed Central PMCID: PMCPMC3196215. doi: 10.1089/omi.2008.0017 PMID: 18416670

70. Aziz RK, Bartels D, Best AA, DeJongh M, Disz T, Edwards RA, et al. The RAST Server: rapid annotations using subsystems technology. BMC Genomics. 2008; 9:75. PubMed Central PMCID: PMCPMC2265698. doi: 10.1186/1471-2164-9-75 PMID: 18261238

71. Moriya Y, Itoh M, Okuda S, Yoshizawa AC, Kanehisa M. KAAS: an automatic genome annotation and pathway reconstruction server. Nucleic Acids Res. 2007; 35(Web Server issue):W182–5. PubMed Central PMCID: PMCPMC1933193. doi: 10.1093/nar/gkm321 PMID: 17526522

72. Quinlan AR, Hall IM. BEDTools: a flexible suite of utilities for comparing genomic features. Bioinformatics. 2010; 26(6):841–2. PubMed Central PMCID: PMCPMC2832824. doi: 10.1093/bioinformatics/btq033 PMID: 20110278

73. Langmead B, Salzberg SL. Fast gapped-read alignment with Bowtie 2. Nat Methods. 2012; 9(4):357–9. PubMed Central PMCID: PMCPMC3322381. doi: 10.1038/nmeth.1923 PMID: 22388286

74. Liao Y, Smyth GK, Shi W. featureCounts: an efficient general purpose program for assigning sequence reads to genomic features. Bioinformatics. 2014; 30(7):923–30. doi: 10.1093/bioinformatics/btt656 PMID: 24227677

75. Love MI, Huber W, Anders S. Moderated estimation of fold change and dispersion for RNA-seq data with DESeq2. Genome Biol. 2014; 15(12):550. PubMed Central PMCID: PMCPMC4302049. doi: 10.1186/s13059-014-0550-8 PMID: 25516281

76. Risso D, Schwartz K, Sherlock G, Dudoit S. GC-content normalization for RNA-Seq data. BMC Bioinformatics. 2011; 12:480. PubMed Central PMCID: PMCPMC3315510. doi: 10.1186/1471-2105-12-480 PMID: 22177264

77. Kuan PF, Chung D, Pan G, Thomson JA, Stewart R, Keles S. A Statistical Framework for the Analysis of ChIP-Seq Data. J Am Stat Assoc. 2011; 106(495):891–903. PubMed Central PMCID: PMCPMC4608541. doi: 10.1198/jasa.2011.ap09706 PMID: 26478641

78. Bailey TL, Boden M, Buske FA, Frith M, Grant CE, Clementi L, et al. MEME SUITE: tools for motif discovery and searching. Nucleic Acids Res. 2009; 37(Web Server issue):W202–8. PubMed Central PMCID: PMCPMC2703892. doi: 10.1093/nar/gkp335 PMID: 19458158